

Cheng-Ta Chen and Chun-Hsien Wu

National Taiwan Normal University, Dept. of Earth Sciences, Taipei, Taiwan

1. INTRODUCTION

The physical basis for atmospheric predictability on seasonal time scales resides primarily on the notion that slowly varying anomalous lower boundary forcing can have significant impact on atmospheric development (Charney and Shukla, 1981; Palmer and Anderson, 1994). Such external forcing is generally thought to be associated with sea surface temperature (SST) anomalies. They can indeed be predicted, either using coupled dynamical models (e.g., Cane, 1991; Barnston et al., 1994; Ji et al., 1994) or statistical models (e.g., Ward et al., 1993; Barnston et al., 1994). Further potential sources of predictive skill, for example, long-lived anomalies in soil moisture and snow cover, are believed to be much less important and are neglected through much of this study.

It is clearly important to be able to access where on the global atmospheric variations are sufficiently affected by oceanic forcing to enable practical seasonal prediction. This requires measurements of atmospheric potential predictability. Recently, potential predictability has been measured using an ensemble of climate simulations, where all are forced by the same observed interannually varying SSTs but started from different initial atmospheric conditions (Kumar and Hoerling, 1995; Rowell, 1998; Brankovic and Palmer, 2000). For predictability study, the sensitivity to initial atmospheric conditions can be used to quantify the random component of interannual variability, whereas the relative similarity (or lack of it) between ensemble members can be used to quantify the potentially predictable component of variance. However, this type of measure calculated from all possible SST states provide little guidance to the expected level of atmospheric prediction skill of individual events. It is important to go beyond the gross measures and understand the predictability limits at different phase and amplitude of ENSO cycle.

In this regard, Chen and Van den Dool (1997) use anomaly pattern correlation (APC) between all possible pair of simulations selected from ensemble members as a measure to gauge the level of predictability. Their finding indicates that during El Niño and La Niña phase of ENSO cycle than during the ENSO inactive period. Furthermore, the predictability is signifi-

cant higher during El Niño than La Niña. There is also large seasonality of predictability for both warm and cold phases of ENSO. Another study by Kumar and Hoerling (1998) use the ratio of seasonal mean SST-forced signal and the internally generated seasonal mean noise to measure potential predictability associated with different phases of ENSO. They also conclude that simulated atmospheric signals were stronger in the extreme warm phases compared to extreme cold phases of ENSO cycle.

It is commonly believed that lower boundary conditions dominate interannual variability in the tropics and major monsoon systems. Therefore, the atmospheric variability is more predictable in those regions. But is there any regional differences? For example, would one expect the circulation over the equatorial eastern Pacific to be more predictable than the tropical western Pacific warm pool. Further, one might also question whether the short-term climate predictability is the same throughout the year. In particular, how does the annual cycle influence the relative impact of anomalous lower-boundary forcing?

The current study examines the potential for seasonal predictability over the Pacific-North American (PNA) and Asian Monsoon regions. The analysis aims to highlight the dependence of the atmospheric signal on amplitude and phase of equatorial SST anomalies. The role of annual cycle's phase is also discussed.

2. DATASETS AND METHODS

2.1 GCM experiments

The model version used for the integrations was ECHAM4 with semi-Lagrangian dynamics at T42L19 resolution. Detail description of the model characteristics can be found in Roeckner et al. (1996). A 10-member ensemble of experiments has been generated for the 1956-1999 period using observed SST and sea ice data compiled for the Atmospheric Model Intercomparison Project (AMIP, Gates, 1992) project. They differ from each other only in the atmospheric initial conditions, and each realization has the same evolving global SST boundary conditions. The model output was archived every 12 hours at 00 and 12 UTC, and monthly averages were derived from such daily data. The 3-month running averages are applied to the above monthly means. Therefore, the monthly values discussed later representing the 12 overlapping 3-month seasons.

Corresponding author address: Cheng-Ta Chen,
National Taiwan Normal Univ., Department Of Earth
Sciences, 88, Sec. 4, Ting-Chou Rd., Taipei, Taiwan,
; e-mail: chen@rain.geos.ntnu.edu.tw

2.2 Measure of signal and noise

An analysis of the climate signal and climate noise for each season in the 44-yr record is performed using the results from the model simulations (Kumar and Hoering, 1998).

Let $X_{i\alpha}$ denotes the simulated seasonal mean anomaly for the year α and realization i . The ensemble mean anomaly averaged over all realizations is defined as

$$\bar{X}_\alpha = \frac{1}{10} \sum_{i=1}^{10} X_{i\alpha} \quad (1)$$

For a particular year, each ensemble member is subjected to the same SST forcing, and the departures of individual realizations from the ensemble mean arise due to the internal variability, or climate noise. This noise is measured by the mean spread \bar{Y}_α averaged over all realizations:

$$\bar{Y}_\alpha = \frac{1}{10} \sum_{i=1}^{10} (X_{i\alpha} - \bar{X}_\alpha)^2 \quad (2)$$

The climate signal defined by (1) and climate noise defined by (2) will depend on the particular SST. In the results of section 3, root-mean-square (rms) area averages of the signal and the noise will be presented. If $\langle \rangle$ denotes an area average, then the rms of

the signal and the noise are defined by $\langle \bar{X}_\alpha^2 \rangle^{1/2}$ and $\langle \bar{Y}_\alpha \rangle^{1/2}$, respectively.

2.3 Analysis methods

As a concise way to summarize the large volume of model data on signal and noise for all SST states during 1956-1999, a graphical representation followed Kumar and Hoering (1998) is used as illustrated in Fig. 1. It shows the seasonal variability of the tropical Pacific SST anomalies during 1956-99 for an area averaged over the NINO3.4 region (5N-5S, 170W-120W). It well represents the phase and amplitude of the past ENSO cycles (Trenberth, 1997). Each bar in the graph corresponds to a 3-month mean, and the individual events have been ranked from the largest warm events on the left hand side to the largest cold events on the right-hand side. The analysis is repeated for the 12 overlapping seasons beginning with December, January, and February and ending with November, December, and January. It is easily seen that SST anomalies are largest in the northern winter season and that warm and cold events aquire comparable peak amplitudes. The model results in section 3 are also arranged according to the ranked amplitude of the SST anomaly. When displayed in this manner, the dependence of the atmospheric signal and noise on the amplitude and phase of ENSO cycle is readily identified. The sensitivity to the annual cycle can aslo be examined in the same plot.

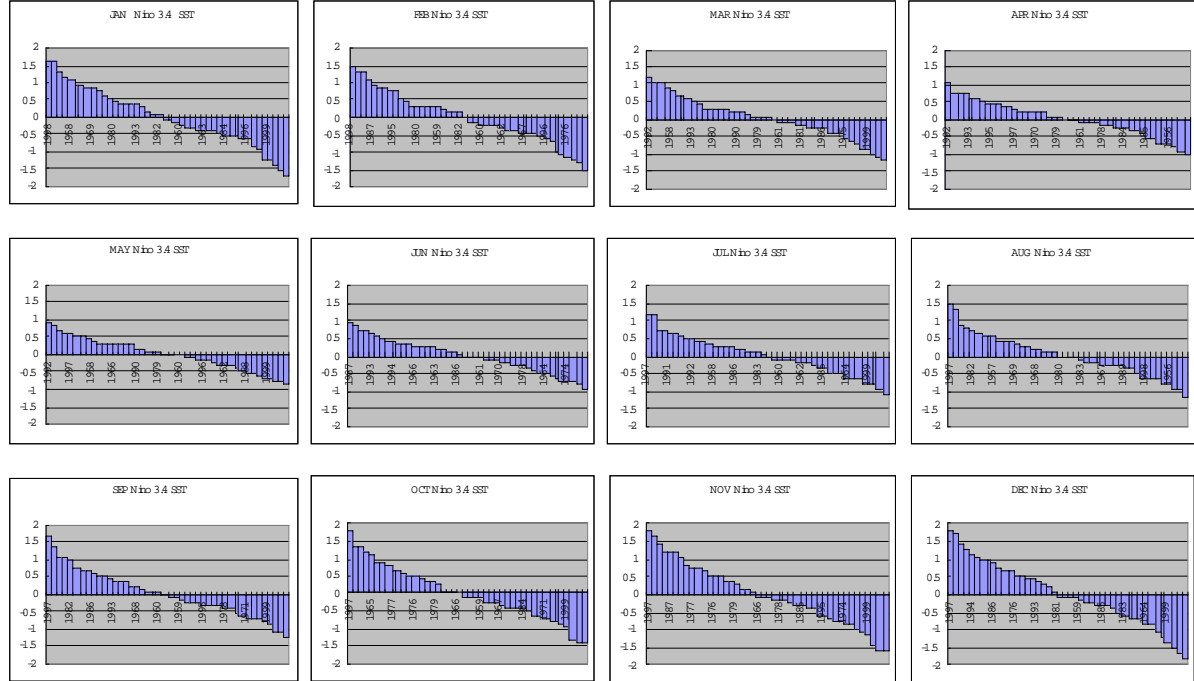


Fig. 1 Sesonal mean sea surface temperature (SST) anomalies during 1956-99 for the NINO 3.4 region (5N-5S, 170W-120W). Each bar denotes the amplitude of the SST anomaly during the 44-yr record, ranked from the largest warm events on the left-hand side to the largest cold events on the right-hand side. the analysis is performed for each of the 12 overlapping 3-month seasons, and the center month of each season is indicated. Unit are $^{\circ}\text{C}$.

3. RESULTS

A limited set of variables are analyzed to assess ENSO's effect on the atmospheric seasonal predictability. They have been chosen to highlight the chain that links the tropical Pacific SSTs and the climate system over the PNA and Asian Monsoon regions. Figure 2. is the warm minus cold composite mean sea level pressure (MSLP) from the six most prominent warm and cold events based on NINO3.4 SST anomalies. There are four highlighted boxes in Fig. 2. Here we will discuss the two boxes located in the northern hemisphere, PNA region (20° - 70° N, 180° - 60° W) and Asian Monsoon region (EQ - 45° N, 90° E- 160° W). The regions are chosen based on the response of atmospheric circulation to the ENSO

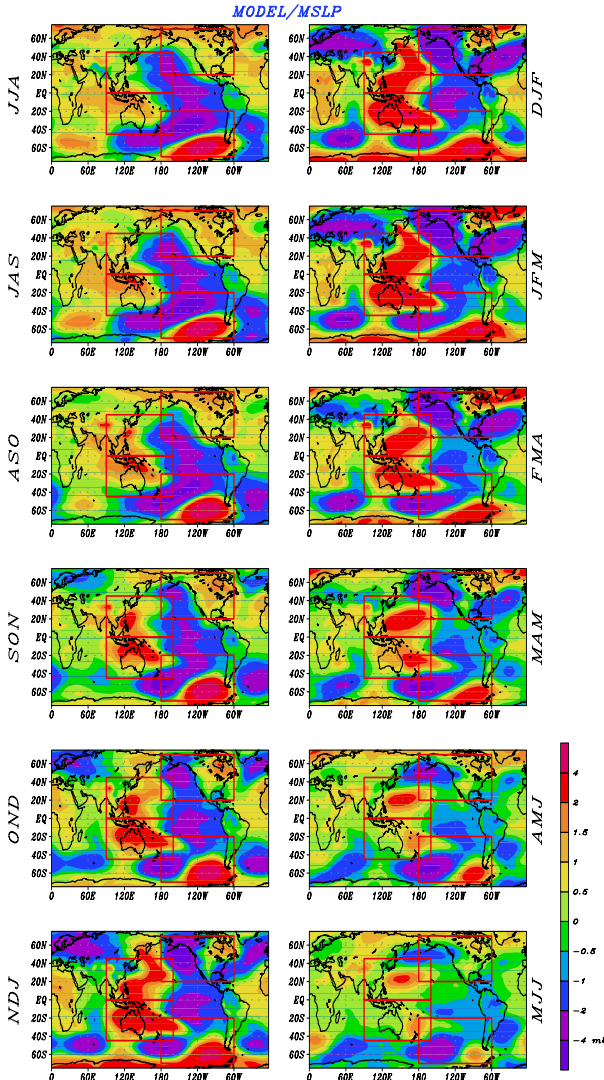


Fig 2. Warm minus cold composite of mean sea level pressure for 12 overlapping 3-month seasons of before and after mature phase of the selected 6 most prominent ENSO events.

forcing. It can be expected that these regions tend to have larger signal based on our definition in section 2.2. It is also important to bear in mind that the results based on the perfect-model approach used herein will be sensitive to the GCM applied.

3.1 Signal and noise over PNA region

Linked with ENSO events and tropical circulation anomalies, there is a characteristic wave pattern whose great circle trajectory leads to center-of action over the North-Pacific and North American region (Horel and Wallace, 1981). This teleconnection pattern is well represented in ECHAM. We will focus on the model's signal over PNA region during each event in 1956-1999 separately. This displayed in Fig. 3 in term of the rms 500-mb-height anomaly area averaged for the region 20° - 70° N and 180° - 60° W.

The signals are slightly higher during the warm events compared to cold events, especially in December and January. The asymmetric response is smaller than the similar study by Kumar and Hoerling (1998) with NCEP model. One can also discern a quasi-linear increase of that signal with the SST amplitude in winter and spring. The largest extratropical signals appear in late winter and early spring; the summer and fall signals are a factor of 2 weaker when the SST anomalies are relatively small. Summer and fall signals exhibit little sensitivity to the amplitude of NINO3.4 SST anomaly.

Similar to the behavior of the signal, a strong seasonal cycle of the climate noise in the extratropical 500-mb heights occurs (Fig. 4), although there is very little dependency on the anomalous SST state itself. The extratropical climate noise is normally greater than climate signal in most of years between 1956-99 and through different 3-month season. Only for the strongest warm and cold events in winter, the signal over PNA regions exceed the noise in the ECHAM model simulations.

Using the signal-to-noise ratio as one measure of potential for seasonal predictability, the seasonal variation of this ratio is evident. It is true even for the year without strong ENSO signal. This is because the seasonal change in climate signal over PNA region is stronger than climate noise. The noise level in summer time is still quite high. If we average the annual cycle of the climate signal and noise for the six strongest warm and cold events to obtain the potential seasonal predictability for El Niño and La Niña phase of ENSO cycle, the ratio is larger in El Niño phase in winter and spring. Climate signal for La Niña period in spring is actually comparable to El Niño period. However, the noise level of El Niño in winter and spring is lower compared to all other years.

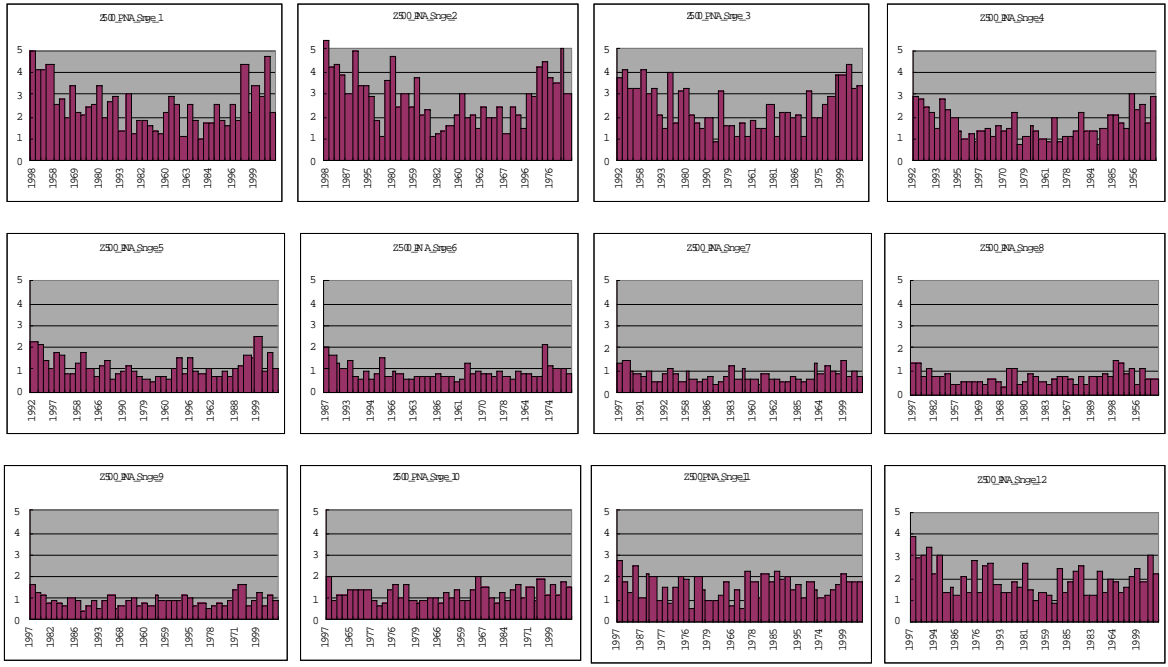


Fig 3. Root-mean-square (rms) signal of the 500-hpa ensemble mean height anomaly. The rms is calculated over PNA region. For each 3 month season, the rms height anomaly is arranged according to the ranked amplitude of SST anomaly in Fig. 1. Units are dm.

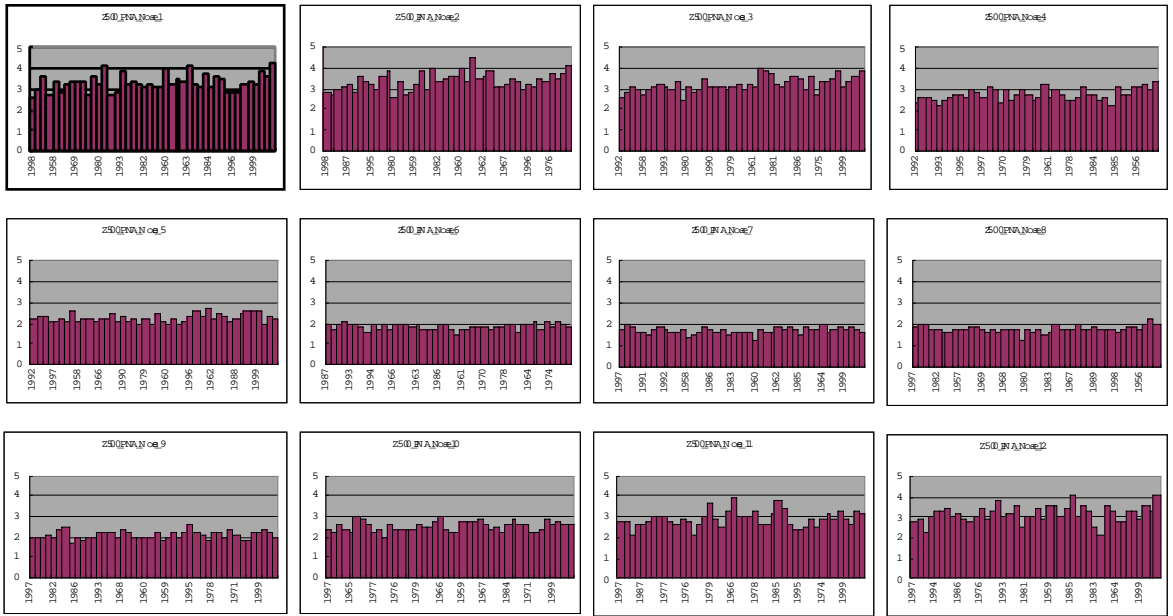


Fig 4. Root-mean-square (rms) noise of the model simulated 500-hpa height anomaly during the 1956-1999. For a given SST state, the atmospheric noise is defined as the departure of the individual simulation from the ensemble mean. The rms is calculated over PNA region. For each 3 month season, the rms height anomaly is arranged according to the ranked amplitude of SST anomaly in Fig. 1. Units are dm.

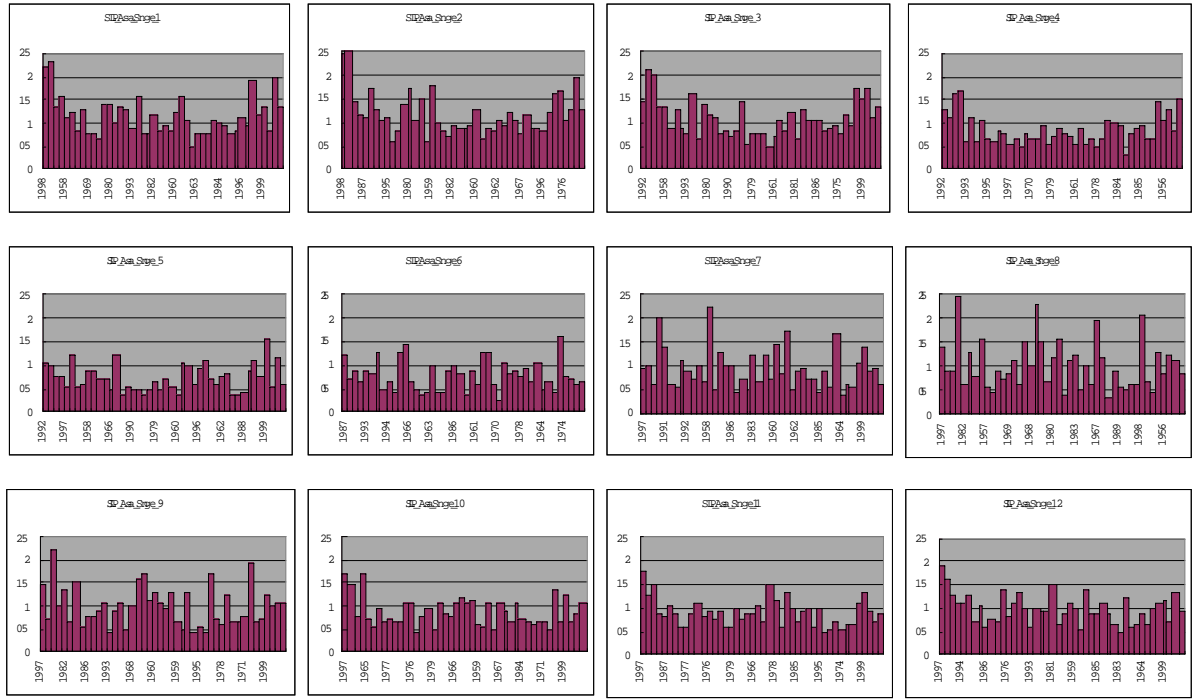


Fig 5. Same as Fig. 3, but for the rms signal of the ensemble mean MSLP anomaliy. The rms is calculated over Asian/Pacific Monsoon region (EQ-45N, 90E-160W). Units are mb.



Fig 6. Same as Fig. 4, but for the rms noise of the model simulated MSLP anomaliy. The rms is calculated over Asian/Pacific Monsoon region (EQ-45N, 90E-160W). Units are mb.

3.2 Signal and noise over Asian/Pacific Monsoon region

The impact of ENSO on the atmospheric and ocean conditions in the Asian/Pacific Monsoon region is discussed in Lau and Nath (2003). It is found that a prominent sea level pressure anomaly over the South China Sea and subtropical northwestern Pacific is positive during the warm events. The wind anomaly in the northwestern portion of this anomalous anticyclone opposes the northeasterly winter monsoon over the East Asian coast, thus leading to warm SST anomalies in that region and above-normal rainfall over southern China. Next we will examine the potential predictable signal over the region and compared to the noise level of the system.

Fig. 5 is the rms mean sea level pressure (MSLP) anomaly area averaged for the region EQ-45°N and 90°E-160°W. The signals are larger during the warm events compared to cold events in late winter and early spring. The signals do not increase with the SSTA amplitude. The signals are relatively weak in the last spring (April, May, June). The summer and fall signals remain similar to winter season. Summer signals exhibit little sensitivity to the amplitude of NINO3.4 SST anomaly.

The seasonal cycle of the climate noise in the MSLP over Asian/Pacific monsoon region is weak. (Fig. 6). The noise levels in summer and winter are slightly larger than in spring and fall season. It also shows no dependency on the anomalous SST state. The Asian/Pacific climate noise is normally greater than climate signal in most of years between 1956-99 and through different 3-month season. Only for the strongest warm events in winter, the signal exceed the noise. Occasionally signal in summer can be larger than noise. But it is not related to the amplitude or sign of SST anomalies.

Using the signal-to-noise ratio as one measure of potential for seasonal predictability, the seasonal variation of this ratio relatively weak. Only in late spring the reduction of climate signal lead to decrease of seasonal predictability, especially for the El Niño years. Comparing the potential seasonal predictability for El Niño and La Niña a phase of ENSO cycle, the ratio is larger in El Niño phase for all the seasons.

Acknowledgements

This work is supported by National Science Council of Taiwan under grants NSC 89-2111-M-003-001, NSC 90-2111-M-003-002-AP1, and NSC 91-2111-M-003-001.

4. REFERENCE

Barnston and Coauthors, 1994: Long-lead seasonal forecasts- Where do we stand? *Bull. Amer. Meteor. Soc.*, **75**, 2097-2114.

Brankovic, C., and T. N. Palmer, 2000: Seasonal skill and predictability of ECMWF PROVOST ensembles. *Q. J. R. Meteorol. Soc.*, **126**, 2035-2067.

Cane, M. A., 1991: Forecasting El Niño with a geographical model. *Teleconnections Connecting World-Wide Climate Anomalies*. M. Glantz, R. Katz, and N. Nicholls, Eds., Cambridge University Press, 345-369.

Charney, J. G., and J. Shukla, 1981: predictability of monsoons. *Monsoon Dynamics*, J. Lighthill and R. P. Pearce, Eds., Cambridge University Press, 99-109.

Chen, W. Y., and H. M. Van den Dool, 1997: Atmospheric Predictability of Seasonal, annual, and decadal climate means and the role of the ENSO cycle: a model study. *J. Climate*, **10**, 1236-1254.

Gate, W. L., 1992: AMIP: The atmospheric model intercomparison project. *Bull. Amer. Meteor. Soc.*, **73**, 1962-1970.

Ji, M., A. Kumar, and A. Leetmaa, 1994: A multiseason climate forecast system at the National Meteorological Center. *Bull. Amer. Meteor. Soc.*, **75**, 569-577.

Kumar, A., and M. P. Hoerling, 1995: Prospects and limitations of seasonal atmospheric GCM predictions. *Bull. Amer. Meteor. Soc.*, **76**, 335-345.

Kumar, A., and M. P. Hoerling, 1998: Annual cycle of Pacific-North American seasonal predictability associated with different phases of ENSO. *J. Climate*, **11**, 3295-3308.

Lau, N.-G., M. J. Nath, 2003: Atmosphere-Ocean Variations in the Indo-Pacific Sector during ENSO Episodes. *J. Climate*, **16**, 3-20.

Horel, J. D., and J. M. Wallace, 1981: Planetary-scale atmospheric phenomenon associated with the Southern Oscillation. *Mon. Wea. Rev.*, **109**, 2080-2092.

Palmer, T. N., and D. T. L. Anderson, 1994: The prospects for seasonal forecasting - A review paper. *Q. J. R. Meteorol. Soc.*, **120**, 755-793.

Roeckner, E., K. Arpe, L. Bengtsson, M. Christoph, M. Claussen, L. D menil, M. Esch, M. Giorgetta, U. Schlese, U. Schulzweida, 1996: *The atmospheric general circulation model ECHAM4: Model description and simulation of present-day climate*. Report 218, Max-Planck-Institut für Meteorologie, Hamburg, Germany, 90pp.

Rowell, D. P., 1998: Assessing potential seasonal predictability with an ensemble of multidecadal GCM simulations. *J. Climate*, **11**, 109-120.

Trenberth, K. E., 1997: The Definition of El Niño. *Bull. Amer. Meteorol. Soc.*, **78**, 2771-2777.

Ward, M. N., C. K. Folland, K. Maskell, A. Colman, D. P. Rowell, and K. Lan, 1993: Experimental seasonal forecasting of tropical rainfall at the UK Meteorological Office. *Prediction of interannual Climate Variations*, Springer-Verlag, 197-216.